Pergamon

Int. J. Heat Mass Transfer. Vol. 40, No. 11, pp. 2525–2537, 1997

Printed in Great Britain
0017-9310/97 $17.00+0.00

PII: S0017-9310(96)00318-3

Detailed heat transfer distributions in two-pass square channels with rib turbulators

SRINATH V. EKKAD and JE-CHIN HAN†

Turbine Heat Transfer Laboratory, Department of Mechanical Engineering, Texas A&M University, College Station, TX 77843-3123, U.S.A.

(*Received* 16 *April* 1996 *and in final form* 4 *September* 1996)

Abstract—Detailed Nusselt number distributions are presented for a two-pass square channel with one ribbed wall. This wall of the channel is sprayed with thermochromic liquid crystals, and a transient test is run to obtain the local heat transfer coefficients. Results are presented for Reynolds numbers ranging from 6000 to 60 000. The rib height-to-hydraulic diameter ratio is 0.125; the rib pitch-to-height ratio is 10; and the rib configurations are 90° parallel, 60° parallel, 60° V, and 60° broken V. Detailed measurements are presented in the first pass, before the 180° turn, in the turn region, after the turn, and further downstream in the second pass. The detailed distributions provide a clear understanding of the secondary flows induced by the 180° turn and the rib turbulators. © 1997 Elsevier Science Ltd. All rights reserved.

INTRODUCTION

Heat transfer augmentation inside cooling channels is achieved by using repeated ribs as turbulence promoters. The periodic ribs break the laminar sublayer and create local wall turbulence due to flow separation and reattachment between the ribs, greatly enhancing the heat transfer. Several researchers have studied the heat transfer and friction characteristics in straight channels. References [1–3] studied the effects of flow Reynolds number and rib geometry on heat transfer and pressure drop in the fully developed region of a uniformly heated square and rectangular channels. Further studies [4–7] showed that angled ribs provide better heat transfer enhancement than transverse ribs. References [8–11] presented heat transfer results for parallel, broken and V-shaped ribs. All of the above studies had channels with two opposite ribbed walls. References [12, 13] reported heat transfer results for one ribbed wall straight channels. Most of the above studies used heater plates and thermocouples for heat transfer measurements. Reference [10] used a heat/mass transfer analogy to study local heat transfer distribution. Recently, ref. [14] presented heat transfer and friction results in rectangular channels with varying number of ribbed walls. They studied heat transfer in channels with one, two, three and four walls with rib turbulators. They reported that increasing the number of ribbed walls not only increases heat transfer enhancement but also increases friction in the channels.

Internal coolant passages in a turbine blade are serpentine with several sharp 180° turns connecting straight sections. References [15–19] presented heat transfer results for smooth and ribbed multi-pass channels. Reference [15] used heaters and thermocouples to measure heat transfer whereas all the other studies for two- or three-pass channels used a heat-/mass transfer analogy to measure local heat transfer distributions. They reported that the local Sherwood numbers on ribbed walls were 1.5–6.5 times those for a fully developed flow in a smooth square channel. They also reported that a 60° angled rib produces higher enhancement compared to 45° and 90° ribs. Reference [18] reported that the combined effects of the rib angle, rib orientation, and the sharp 180° turn significantly affect the local mass transfer distributions. The mass transfer technique provides local heat/mass transfer distributions along three axial lines on the channel surface. Also, the previous studies for two-pass channels using the mass transfer technique provided results for only smooth, transverse (90°) and angled (45°, 60°) ribs.

The first group of the above-mentioned studies (refs. [1–9, 11–13]) focused on the effect of many rib geometries on the heat transfer and friction in straight rectangular channels using the standard heater plates/foils and thermocouple technique. They provided regional heat transfer enhancement and a pressure drop penalty, and their correlations in ribbed channels. However, they do not provide the detailed heat transfer coefficient distributions in the ribbed channels. The second group of studies (refs. [16–18]) focused on the effect of several rib orientations on the heat/mass transfer enhancement in two- or three-pass square channels using the naphthalene sublimation technique. They provide a little bit more information about the local heat/mass transfer distributions. However, they still do not provide the required detailed

† Author to whom correspondence should be addressed.

NOMENCLATURE

D	square channel width or height	Re	Reynolds number ($\rho VD/\mu$)
e	rib height	t	time of liquid crystal color change
k	thermal conductivity of test surface material	T_i	initial temperature of test surface
k_a	thermal conductivity of air	T_w	liquid crystal color change temperature
L	length of each pass	T_m	mainstream temperature
N	number of step changes on the chart recorder output	V	mainstream flow velocity
Nu	local Nusselt number (hD/k_a)	X	axial distance from center of the channel.
Nu_0	Nusselt number from correlation for a straight channel, $0.023Re^{0.8}\ Pr^{0.4}$	Greek symbols	
$\bar{Nu}$	spanwise or regional averaged Nusselt number	α	thermal diffusivity of test surface material
P	rib pitch	μ	dynamic viscosity of air
Pr	Prandtl number of air	ρ	density of air.

heat transfer coefficient distributions between ribs, on the ribs, in the 180° turn region, and in the second pass of the two-pass channel. In the turbine blade internal cooling design, it is important to know the detailed heat transfer coefficient distributions on the ribbed walls, particularly in the 180° turn region, in order to prevent the local hot spots in the coolant passages. This is the reason detailed heat transfer information is still an important concern in the advanced turbine blade cooling design.

The present study focuses on the detailed heat transfer coefficient measurements for smooth and various rib-roughened two-pass channels using a transient heat transfer technique with a liquid crystal coating on the test surfaces. The detailed heat transfer distributions help understand the flow physics in the two-pass ribbed channels such as separation, reattachment and secondary flow due to rib angle, flow turning and impingement in the 180° sharp turn region, and flow redevelopment after the 180° turn in the second pass of the two-pass channel. The detailed heat transfer distributions help understand the heat transfer enhancement process and provide better rib geometry/orientation for turbine blade internal cooling design. Reference [20] used the transient liquid crystal image technique in the sharp 180° turn region of a two-pass square channel with smooth walls. A similar technique will be extended for the present study.

The objective of this study is to provide detailed heat transfer coefficient distributions for a two-pass square channel with various rib configurations. Results are presented for a smooth channel and four ribbed channels with 90° parallel ribs, 60° parallel ribs, 60° V ribs, and 60° broken V ribs. Four flow Reynolds numbers ranging between 6000 and 60 000 are studied for each channel. This study focuses on a two-pass channel with only one ribbed wall. All the results are presented for the ribbed wall only.

TEST APPARATUS

Figure 1 presents a schematic of the experimental setup. The experimental setup consists of an image-processing system, a flow circuit, and the test section. The image-processing system consists of an RGB camera to view the liquid crystal coated test surface. The camera is connected to a color frame grabber board placed inside the PC. The frame grabber board is programmed through a software package to analyze the color changes during the transient test. A monitor is also connected to the frame grabber board for reference.

The flow circuit consists of a compressor-based air supply. The air passes through a standard orifice meter which measures the mass flow rate. Air then passes through an in-line heater and a three-way ball diverter valve. The heater input, controlled by a transformer, heats the air to the required temperature. The ball diverter valve routes the air away from the test section when the test is not in progress. A transient test is initiated by switching the valve and letting the hot air into the test section.

Figure 2 presents the front view of the test section, indicating the test wall, rib spacing, rib size, and channel dimensions. The test section is a two-pass channel with a 5.08 cm square cross-section. Each pass is 60.96 cm long, with an L/D ratio of 12. The whole test section is made of plexiglass. The back wall is made of black plexiglass and sprayed with liquid crystals on the inside. The liquid crystal coated surface is observed through the transparent opposite wall. The ratio of the divider wall thickness to the channel width

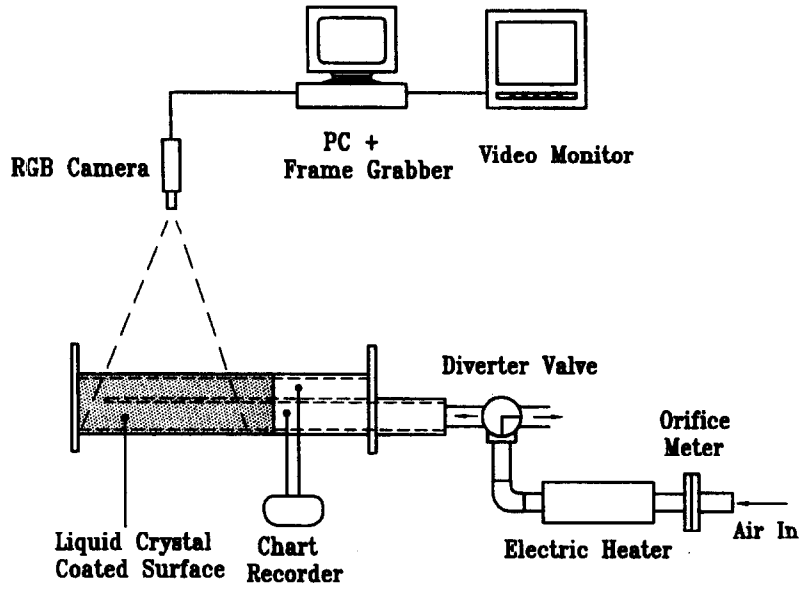

Fig. 1. Experimental setup.

(t/D) is 0.25. The thickness of the plexiglass wall is 1.27 cm.

For the rib-roughened ducts, black plexiglass ribs were attached to the test surface using double-sided tape. Liquid crystals were sprayed after attaching the ribs to the surface. Four rib configurations, 90° parallel, 60° parallel, 60° V, and 60° broken V, were studied. Figure 2 also presents the rib configurations on the channel wall. The rib height-to-channel width (e/D) is 0.125, and the rib pitch-to-height ratio (P/e) is 10. A 90° rib was placed along the divider wall in the middle of the 180° turn. This rib was common for all the rib configurations. The axial distance (X) is measured from the middle of the turn. Positive X indicates second pass and negative X indicates first pass.

DATA REDUCTION

The liquid crystal coated surface is suddenly exposed to a hot mainstream, and the color change temperature at each pixel location on the test surface is registered by the image-processing system. The local heat transfer coefficient (h) over the test surface can be obtained by assuming one-dimensional transient conduction over a semi-infinite solid. The surface temperature response into the semi-infinite surface with a convective boundary condition at the surface is shown as

$$\frac{T_w - T_i}{T_m - T_i} = 1 - \exp\left(\frac{h^2 \alpha t}{k^2}\right) \operatorname{erfc}\left(\frac{h\sqrt{\alpha t}}{k}\right) \quad (1)$$

where T_w is the color change temperature from red to green during the transient test, T_i is the initial temperature of the test surface, T_m is the oncoming time-dependent mainstream temperature, and t is the time of color change to green at any location. Test conditions are set such that the time of color change on the surface is between 10–80 s. This enables the validity of the semi-infinite solid assumption on the test surface.

The chart recorder measures the time-dependent variation of the mainstream temperature in the middle of each pass. The axial temperature in the channel is interpolated from the two measured locations. Although the axial temperature variations in the channel measured region is not linear, especially in the turn region, this method helps increase the accuracy of the local mainstream temperature prediction compared to using a single temperature for the entire channel. Figure 3 presents the typical time–temperature history for the mainstream at the inlet and outlet of the measured region. There is a temperature drop from the inlet of the measured section to the outlet through the 180° sharp turn region. The local mainstream temperature at any axial location on the test surface is linearly interpolated between the inlet and outlet measured temperatures to improve accuracy in the heat transfer coefficient calculation. Since the local mainstream temperature (T_m) at any location is a function of time, the solution in equation (1) has to include the time-variance of the mainstream temperature. The time history of the mainstream temperature is simulated as a series of time step changes. The time step changes of the mainstream temperature at every location are included in the solution for heat transfer coefficient using the Duhamel's superposition theorem. The solution for the heat transfer coefficient (h) at every location is then represented as

$$T_w - T_i = \sum_{j=1}^{N} \left\{1 - \exp\left[\frac{h^2 \alpha (t - \tau_j)}{k^2}\right] \times \operatorname{erfc}\left[\frac{h\sqrt{\alpha(t-\tau_j)}}{k}\right]\right\} [\Delta T_{m(j,j-1)}] \quad (2)$$

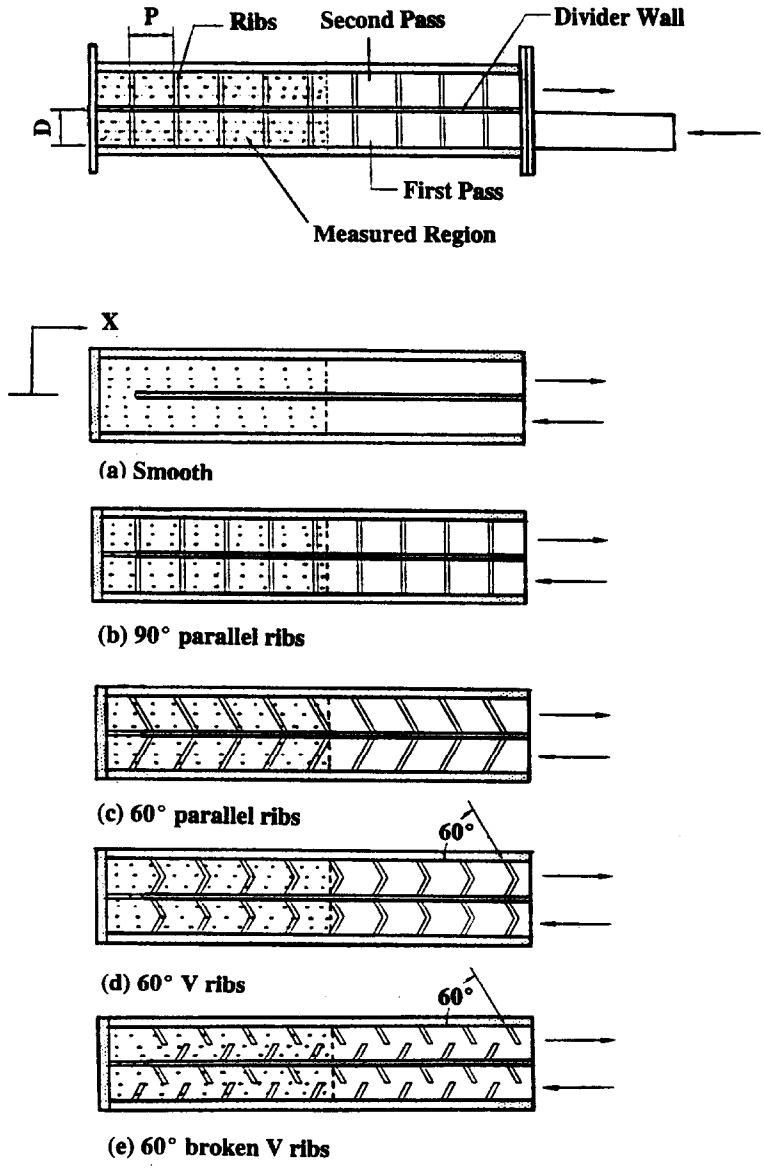

Fig. 2. Test surface geometry with rib configurations.

where $\Delta T_{m(j,j-1)}$ and τ_j are the temperature and time step changes obtained from the chart recorder output. The equation is solved at every point on the surface

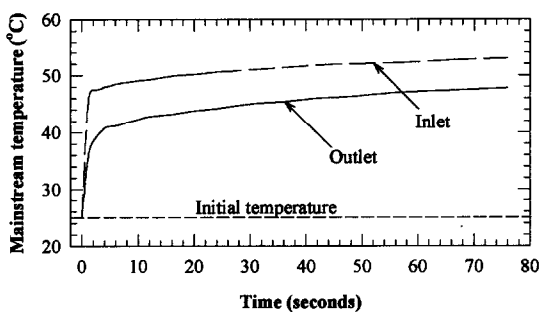

Fig. 3. Mainstream temperature variations during the transient test.

(250 × 90 points) to obtain the local heat transfer coefficient.

Thermochromic liquid crystals are sprayed uniformly on the test surface using an air gun. The coating is a light spray of thickness on the order of 5–10 μm. The main flow is set to the required flow rate and heated to a required temperature. Once the temperature achieves a steady value, the diverter wall is flipped and the hot air is sent over the test surface, causing the liquid crystals to change color. The computer records the time for the liquid crystals to change color to green from the start of the transient test. The measured mainstream temperature from the chart recorder and the computer measured times of color change are used to solve for the local heat transfer coefficient at every location (250 × 90).

The experimental uncertainty in the measurement of the convective heat transfer coefficient (h), based on methodology from ref. [21], is on the order of $\pm 5.9\%$. The individual uncertainties in the measurement of the time of color change (t) is $\pm 2.5\%$, the mainstream temperature (T_m) is $\pm 1.5\%$, the color change temperature (T_w) is $\pm 0.8\%$, and the wall material properties (α, k) are $\pm 5.0\%$. These uncertainties were included in the calculation of the overall uncertainty in the measurement of 'h'.

RESULTS AND DISCUSSION

Detailed Nusselt number ratio distributions

Figure 4(a)–(e) presents the detailed Nusselt number ratio (Nu/Nu_0) distributions for all five cases (smooth and ribbed channels) at $Re = 12\,000$, $30\,000$ and $60\,000$. The fully developed flow Nusselt number (Nu_0) for a smooth square channel is obtained from the Dittus–Boelter correlation for a smooth circular tube. Nusselt number ratios in the entire channel

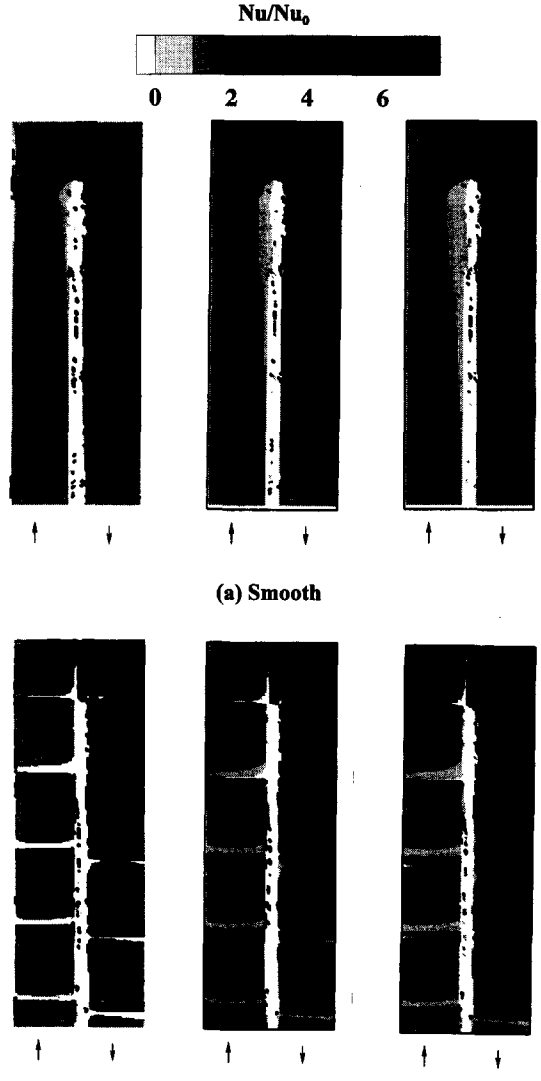

Fig. 4. (a) Detailed Nusselt number ratio distributions for a smooth channel. (b) Detailed Nusselt number ratio distributions for a channel with 90° parallel ribs. (c) Detailed Nusselt number ratio distributions for a channel with 60° parallel ribs. (d) Detailed Nusselt number ratio distributions for a channel with 60° V ribs. (e) Detailed Nusselt number ratio distributions for a channel with 60° broken V ribs. (*Continued overleaf.*)

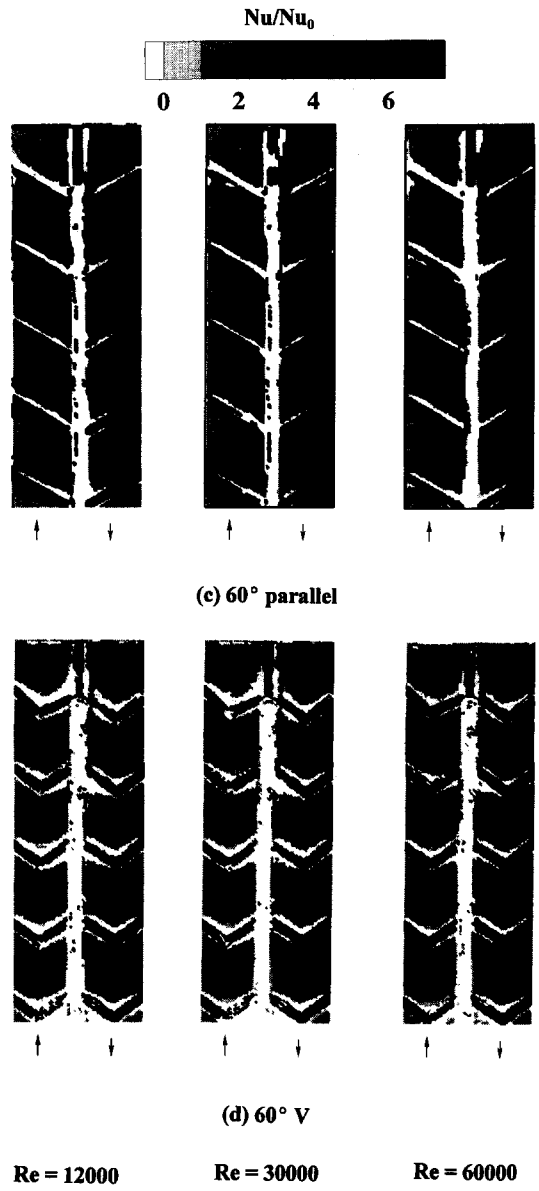

Fig. 4—*Continued.*

decrease with an increase in Reynolds number for all smooth and ribbed channels, as can be observed clearly in the turn and after-turn regions.

Figure 4(a) presents the detailed Nusselt number ratio distributions in a two-pass smooth channel. In the first pass, there is very little spanwise variation. As the flow approaches the 180° turn, the Nusselt number ratio reaches a low value very close to 1.0, which indicates that the flow in the first pass is approaching the fully developed flow condition. The turn effect is three-dimensional and is influenced by the flow separation at the divider tip and the secondary flows induced by the centrifugal forces. Before the turn, the flow tends to move towards the divider wall, producing a small recirculation region near the outer wall. This can be observed as a low heat transfer region. High heat transfer is observed away from the divider wall in the turn region. This may be due to the flow impinging from the first pass before being affected by the 180° turn. As the flow enters the second pass, higher Nusselt number ratios are observed away from the divider wall. This may be due to the centrifugal forces due to the sharp 180° turn causing the flow to impinge on the outer wall. Further downstream into the second pass, Nusselt number ratios decrease as effect of the turn reduces. In addition, the spanwise variations observed in the turn region decrease farther downstream into the second pass.

Figure 4(b) presents the detailed Nusselt number ratio (Nu/Nu_0) distributions in the two-pass channel with 90° parallel ribs. The 90° ribs enhance the heat transfer on the surface compared to a smooth surface.

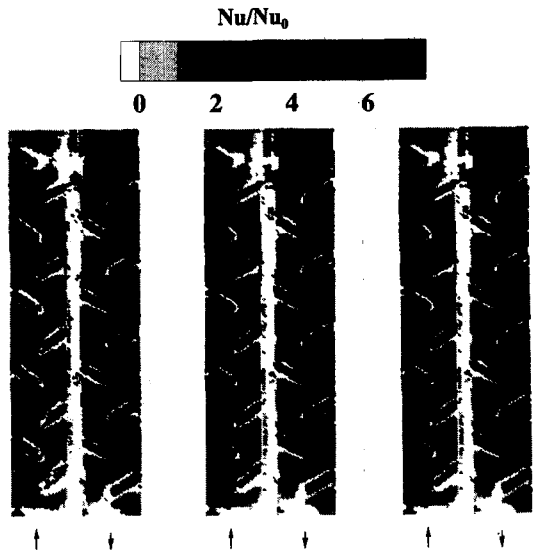

(e) 60° broken V

Re = 12000 Re = 30000 Re = 60000

Fig. 4—*Continued.*

There is greater spanwise and axial variations in the Nusselt number ratio distributions due to the presence of the ribs. Highest Nusselt number ratios are observed on the top of the ribs. The distributions between adjacent ribs appear periodic in the entire channel. Heat transfer is high in the middle region between two ribs, and very low immediately before and after the ribs. In the turn region, heat transfer is enhanced greatly due to the combination of the sharp 180° turn and the 90° ribs. The presence of the ribs appears to reduce the effect of centrifugal forces on the secondary flow and causes lesser impingement on the outer walls. Locally high heat transfer regions are obtained immediately downstream of the ribs in the turn and the second pass. Further downstream into the second pass, Nusselt number ratios decrease with the reduction in the effect of the turn. The heat transfer distribution appears to retain the periodicity between two adjacent ribs about three rib pitches downstream into the second pass.

Figure 4(c) presents the detailed Nusselt number ratio (Nu/Nu_0) distributions in a two-pass channel with 60° parallel ribs. The ribs in the first pass are angled away from the divider wall and the ribs in the second pass are angled towards the divider wall. There is a 90° rib in the turn region. The 60° ribbed channel produces higher enhancement than the 90° ribbed channel. Highest Nusselt number ratios are obtained on top of the ribs in both the passes of the channel. Heat transfer distribution between adjacent ribs is periodic over the entire channel. The secondary flow moves away from the divider wall towards the outer wall in the first pass. Nusselt number ratios decrease from the divider wall to the outer wall in the spanwise direction. In the turn region, Nusselt number ratios are very high due to the combination of the 180° sharp turn and the 90° rib. The centrifugal effect due to the turn on the secondary flow is reduced due to the presence of the ribs. In the second pass, Nusselt number ratios are higher near the outer wall and decrease towards the divider wall. This is due to the angle of the ribs. The secondary flow in the second pass moves from the outer wall towards the divider wall. Nusselt number ratios decrease further downstream as the effect of the turn reduces and distribution becomes more periodic between the ribs.

Figure 4(d) presents the detailed Nusselt number ratio (Nu/Nu_0) distributions in a two-pass channel with 60° V ribs. The direction of the V ribs is shown in Fig. 2. There is a 90° rib in the middle of the turn. The Nusselt number ratios are highest on the top of the ribs. In the first pass, the secondary flows induced by each angled side of the V rib move away from the center of the channel. A high heat transfer enhancement region is obtained along the centerline of the channel. Nusselt number ratios are lower immediately upstream and downstream of each rib in the first pass due to flow separation from the rib, forming two vortices before and after rib corners. A very low Nusselt number region is produced immediately downstream of the last V rib in the first pass due to the separation caused by the additional effect of the turn. The 90° rib in the turn region produces high enhancement immediately downstream of the rib. Further downstream, the Nusselt number ratios in the second pass are higher than those for 90° and 60° ribbed channels. Two secondary flows are generated by the ribs in the second pass. The secondary flow near the outer wall

has higher momentum due to the influence of the centrifugal forces, whereas the secondary flow near the divider tip has lower momentum. A high heat transfer region is produced closer to the outer wall. Further downstream, the effect of the turn reduces and the local Nusselt number ratios decrease. The secondary flows created by the ribs by itself produce much lower enhancement compared to the combined effect of the secondary flows created by the ribs and the sharp 180° turn.

Figure 4(e) presents the detailed Nusselt number ratio (Nu/Nu_0) distributions in a two-pass channel with 60° broken V ribs. Nusselt number ratios are highest on top of the ribs. The broken V ribs are 60° V ribs broken and staggered. There is a 90° rib in the middle of the turn. The heat transfer enhancement in the first pass is limited to the mid-channel region. Highest enhancement is downstream of each rib along the direction of the rib. The distribution in the first pass appears to be serpentine due to secondary flows generated along the broken V ribs. The Nusselt number ratios in the turn region in the first pass are very low. The rib configuration used in the present study reduces the secondary flow velocity, thus reducing heat transfer enhancement. In the turn region in the second pass, heat transfer is enhanced greatly by the 90° rib in the turn. The enhancement in the second pass after-turn region is much higher than the enhancement in the first pass. Nusselt number ratios are higher near the outer wall due to the turn effect. Further downstream, the effect of the turn reduces and the higher heat transfer region moves closer towards the mid-channel region.

Figure 5 presents detailed Nusselt number ratio distributions for $Re = 30\,000$ in the first pass between two adjacent rib pitches ($X/D = -2$ to -5). The Nusselt number ratio between adjacent ribs for all rib configurations is periodic. The secondary flow structures are clearly evident for the 60° parallel, 60° V, and 60° broken V ribs. The region is not affected by the 180° turn downstream. The highest enhancement region between the ribs is dependent on the secondary flow structure produced by the rib configuration. The 60° parallel rib has secondary flow from the divider wall towards the outer wall. The V rib has two secondary flows generated at the tip of the ribs and moving away from the center of the channel. The broken V rib has serpentine secondary flows with highest Nusselt numbers immediately downstream of the ribs.

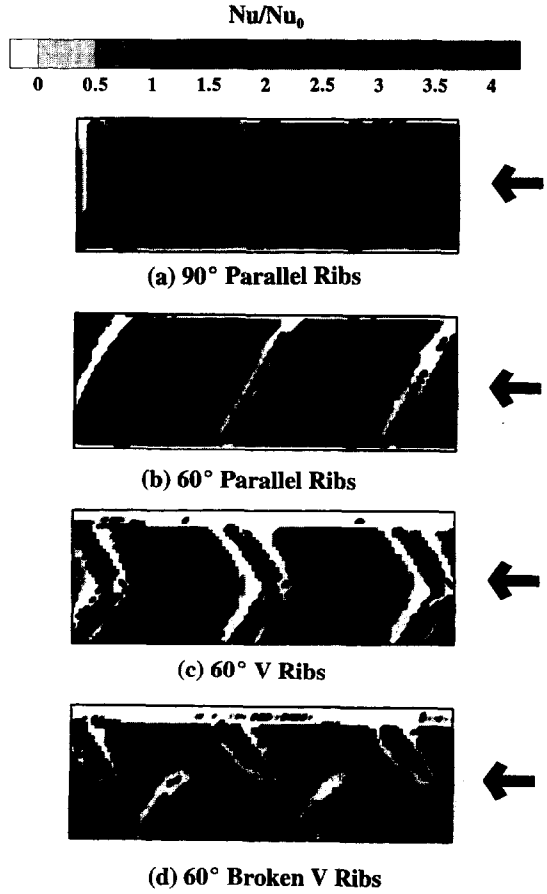

Fig. 5. Detailed Nusselt number ratio distributions in the first pass of the channel at $Re = 30\,000$.

Spanwise heat transfer distributions

Figure 6 compares the spanwise-averaged Nusselt number ($\bar{Nu}/Nu_0$) distributions for each of the five configurations at $Re = 12\,000$ and $60\,000$. The rib locations are indicated by dark squares on the figure for 90° parallel ribs. Nusselt number ratios are lower for $Re = 60\,000$ compared to those for $Re = 12\,000$ as discussed earlier. The smooth surface distributions show very little variations in the distributions. In the first pass, the Nusselt number ratio decreases and is almost equal to 1.0 just before the turn region. Nusselt number ratios increase in the turn region and reach a maximum in the after-turn region in the second pass and decrease further downstream into the second pass.

The ribbed channels show periodic spikes in the spanwise averaged distributions. The Nusselt number ratios are highest on the ribs, and low upstream and downstream of the ribs. The spikes are clearly evident for the 90° ribbed channel. The 90° ribs are along the channel span and the averaging is also along the span. However, for the other ribbed channels, the ribs are at an angle to the channel span due to which the periodic spikes are not very strong. The after-turn region has the highest Nusselt number ratios due to the strong effects of both the 180° sharp turn and the presence of ribs. Further downstream, the effect of the turn reduces. The average Nusselt number over each pass is higher for the 60° parallel and 60° V ribs compared to other configurations. The 60° broken V rib produces similar enhancement levels as the 60° parallel ribs in the first pass. However, they produce much lower enhancement in the turn region compared to all other rib configurations. The spanwise distributions are presented to indicate the axial heat transfer enhancement variations in the entire channel.

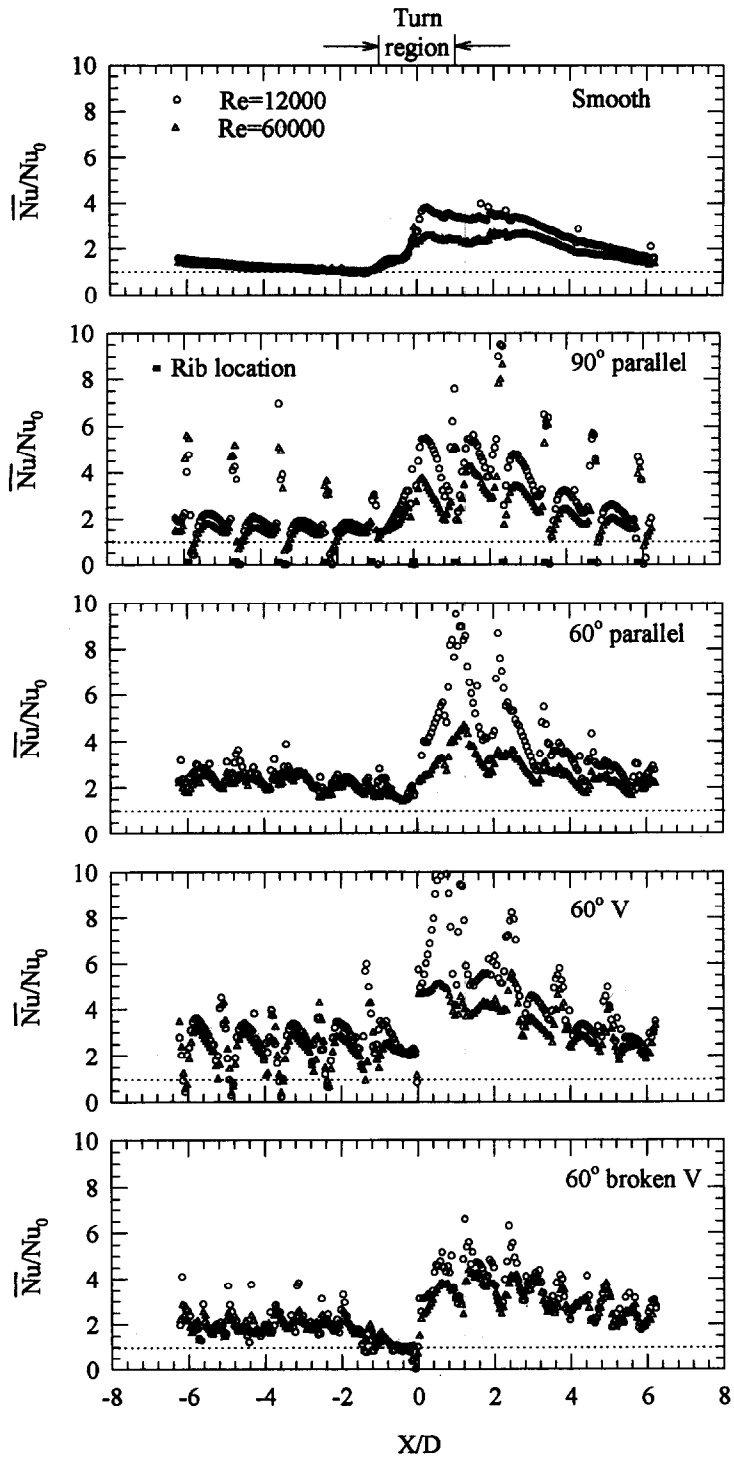

Fig. 6. Spanwise averaged Nusselt number distributions for all five configurations at $Re = 12\,000$ and 60 000.

Regionally averaged distributions

The local Nusselt number ratios are regionally-averaged over every rib pitch, including the rib top on the channel wall in the first pass, in the turn region, and the second pass. Figure 7 presents the effect of rib angle on regionally averaged Nusselt number ratio at each Reynolds number. At $Re = 6000$, all rib configurations produce a similar scale of enhancement in the first pass. In the turn region, 90° ribs produces the highest enhancement. Further downstream in the second pass, Nusselt number ratios for all the ribbed channels decrease as the effect of the turn is reduced.

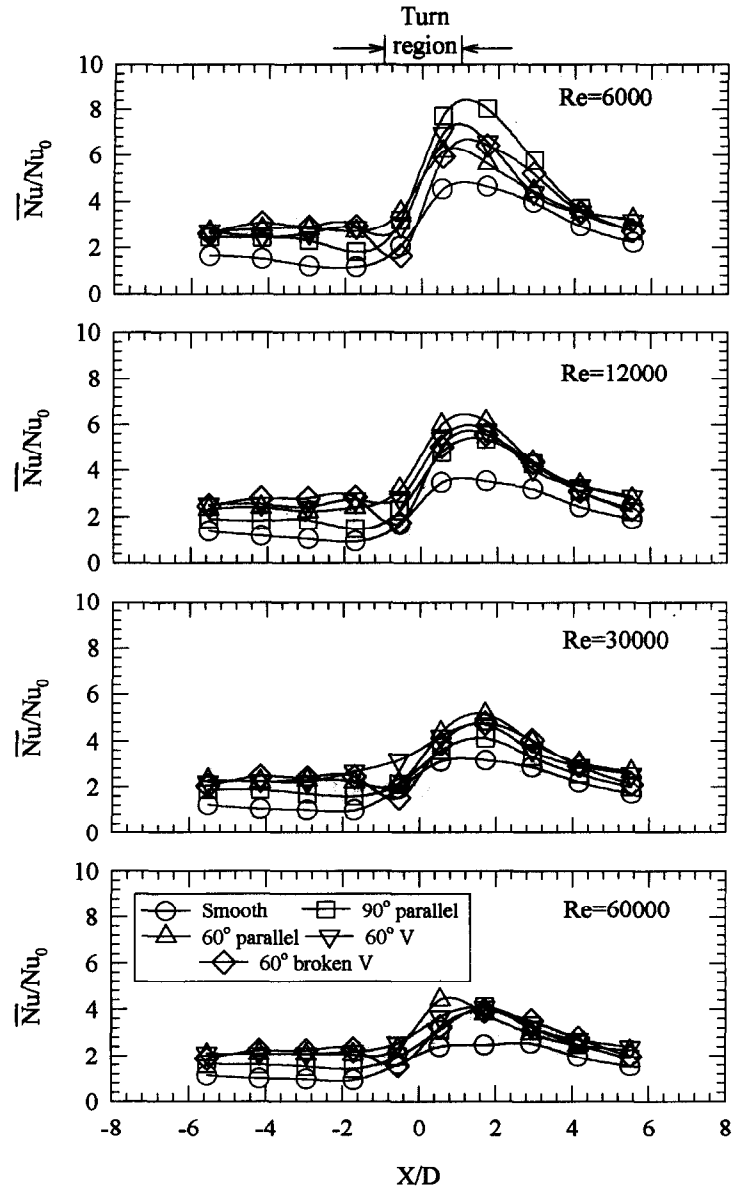

Fig. 7. Effect of rib configuration on regionally-averaged Nusselt number ratio for all four Reynolds numbers.

At $Re = 12000$, 60° broken V ribbed channel produces higher Nusselt number ratios in the first pass compared to other ribbed and smooth channels. However, in the second pass, the Nusselt number ratio for the 60° parallel and 60° V ribs are slightly higher than for the 60° broken V ribbed channel. For higher Reynolds numbers, the effect of various ribs does not produce strong variations in the regionally averaged Nusselt number ratio distributions. Both 60° parallel ribs and 60° V ribs produce similar enhancement. The 60° broken V rib channels produce a very low Nusselt number ratio immediately upstream of the turn for all the Reynolds numbers. This may be due to flow separation and recirculation near the last rib on the first pass [see Fig. 4(e)].

Figure 8 presents the effect of Reynolds number for regionally-averaged Nusselt number ratios in the entire first pass ($X/D = -6$ to -2), in the turn region ($X/D = -2$ to 2), and the entire second pass ($X/D = 2$–6). The Nusselt numbers in the region on the rib top are also included in the averaging. The single value for each region at each Reynolds number represents the overall enhancement in the region due to the ribs. For the first pass, Nusselt number ratios decrease with increase in Reynolds number for all rib configurations and a smooth surface. The 60° broken V ribs produce the highest enhancement in the first pass. The enhancements for the 60° parallel and 60° V ribs are slightly lower than for 60° broken V ribs. For the turn region, Nusselt number ratios show a

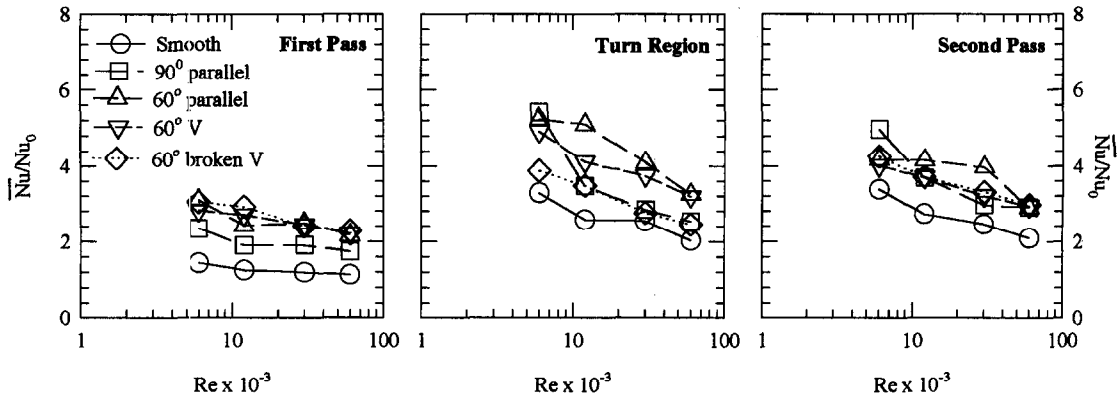

Fig. 8. Effect of Reynolds number on average Nusselt number ratio for each channel region.

stronger decrease with increase in Reynolds number. The 60° parallel ribbed channel produces higher Nusselt number ratios than all the other rib configurations. The 60° V ribbed channel produces slightly lower values. All the ribbed channels have a 90° rib in the middle of the turn. Nusselt number ratios decrease with an increase in Reynolds number for all the channels in the second pass. The 60° V ribbed channel and the 60° broken V ribbed channel produce similar Nusselt number ratios. The 60° parallel ribs produce higher Nusselt number ratios than the 60° V and 60° broken V ribs. For all the three regions, smooth surface Nusselt number ratios are lowest as expected.

Comparisons

The results from the present study have been compared with results obtained by previous investigators. Figure 9(a) compares results for smooth two-pass channels with results from refs. [17] and [19] at $Re = 30\,000$. The results are in good agreement in the first pass. However, the results from present study are much higher in the turn and second pass. References [17] and [19] measured regionally averaged heat transfer coefficient results using a naphthalene sublimation technique compared to the detailed measurements in the present study.

Figure 9(b) compares results from refs. [9] and [14] with the present study for a 90° ribbed channel at $Re = 30\,000$. Both studies ([9, 14]) measured regional averaged heat transfer in straight ribbed channels using thermocouples and heater plates. Results from ref. [9] were for channels with two opposite ribbed walls, and ref. [14] had one side ribbed wall similar to the present study. Both studies show higher Nusselt number ratios compared to results in the first pass.

Figure 9(c) compares results from ref. [8] with the present study for 60° parallel and 60° V ribs at $Re = 30\,000$. Reference [8] presented regional averaged heat transfer for straight channels using thermocouples and heater plates. The present results in the first pass are lower than the results from ref. [8] for both rib configurations. The present results could be lower than the published results due to three main reasons. Firstly, the liquid crystal technique is unable to measure the separated flow region heat transfer immediately downstream of the rib [see Fig. 4(b)–(e)]. The averaging produces lower results due to this low (nearly zero) heat transfer region. Reference [8] has two-sided ribbed walls which causes a 10% higher heat transfer than for a one-sided ribbed wall as in the present study. Since the present study has ribs only on one side, the secondary flows developed may not be as strong as they would be if both the sides were ribbed. Most importantly, refs. [8, 5, 9, 14] used copper ribs on the copper plates in the test channel. Additional heat was removed from the front and back sides of the ribs. This additional rib side area increases the overall heat transfer area by more than 20% of the entire smooth surface area. The present liquid crystal experiments provide heat transfer coefficients between the ribs and the rib top, but do not include heat transfer to the rib sides. Therefore, the present average Nusselt numbers are lower than other studies. The main focus of the present study is to present detailed heat transfer distributions in smooth and turbulated channels which provide valuable insight into the enhancement phenomena caused by secondary flows induced by the ribs and the sharp 180° turn.

CONCLUSIONS

Local Nusselt number distributions are presented for turbulent flow in a two-pass square channel for smooth and ribbed walls using a transient liquid crystal technique. The conclusions based on the results presented are:

(1) Nusselt number ratios in the second pass are nearly 2–3 times higher than for the first pass due to the 180° sharp turn effect in the smooth channel. Nusselt number ratios in the after-turn and the second pass decrease with an increase in Reynolds number.
(2) The 60° parallel, 60° V and 60° broken V ribs

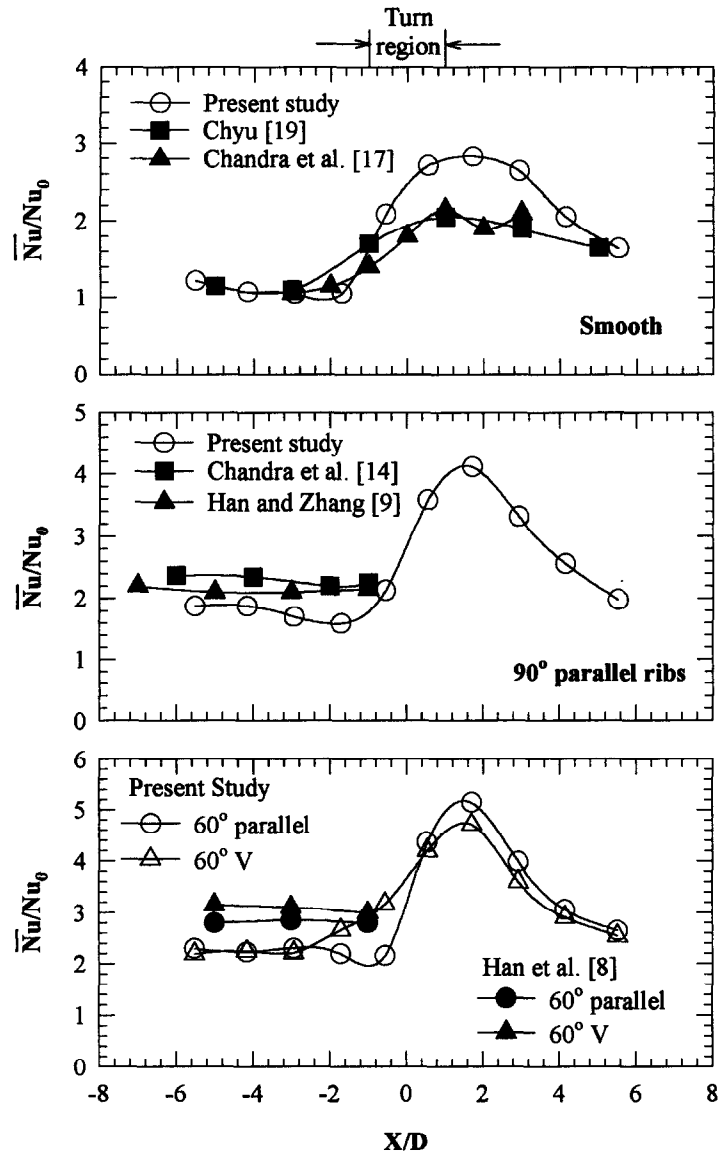

Fig. 9. Comparison of results from present study with published results at $Re = 30\,000$.

produce similar high heat transfer enhancement in the first pass with 60° broken V ribs slightly higher. However, 60° parallel ribs produce higher enhancement in the turn and second pass.

(3) Nusselt number distributions in the first pass are mostly periodic for all ribbed channels between two adjacent ribs. However, the effect of the 180° turn combined with the presence of the ribs produces much higher Nusselt numbers in the after-turn region in the second pass.

(4) Nusselt numbers are highest on the top of the ribs for all ribbed channels. However, Nusselt numbers are lowest immediately before and after the ribs for all ribbed channels.

(5) The present averaged Nusselt numbers show the same trends as the published results for straight channels with metallic ribs. However, the present Nusselt numbers are lower because the rib-increased heat transfer area is not included in the heat transfer coefficient calculations. However, the detailed Nusselt number distributions presented in this study help understand the heat transfer enhancement phenomena due to ribs and the sharp 180° turn. There are no previous publications providing such detailed heat transfer distributions for two-pass channels with various rib turbulators.

Acknowledgements—This paper was prepared with the support of the U.S. Department of Energy, Morgantown Energy Technology Center, Cooperative Agreement No. DE-FC21-92 MC 9061. The technical team of Advanced Turbine Systems at Clemson University is Drs D. B. Fant and L. P. Golan. Their support is greatly appreciated.

REFERENCES

1. Han, J. C., Glicksman, L. R. and Rohsenow, W. M., An investigation of heat transfer and friction for rib-roughened surfaces. *International Journal of Heat and Mass Transfer*, 1978, **21,** 1143–1156.
2. Han, J. C., Heat transfer and friction in channels with two opposite rib-roughened walls. *ASME Journal of Heat Transfer*, 1984, **106,** 774–781.
3. Han, J. C., Park, J. S. and Lei, C. K., Heat transfer enhancement in channels with turbulence promoters. *Journal of Engineering for Gas Turbines and Power*, 1985, **107,** 629–635.
4. Han, J. C., Heat transfer and friction characteristics in rectangular channels with rib turbulators. *ASME Journal of Heat Transfer*, 1988, **110,** 321–328.
5. Han, J. C. and Park, J. S., Developing heat transfer in rectangular channels with rib turbulators. *International Journal of Heat and Mass Transfer*, 1988, **31,** 183–195.
6. Han, J. C., Ou, S., Park, J. S. and Lei, C. K., Augmented heat transfer in rectangular channels of narrow aspect ratios with rib turbulators. *International Journal of Heat and Mass Transfer*, 1989, **32,** 1619–1630.
7. Park, J. S., Han, J. C., Huang, Y. and Ou, S., Heat transfer performance comparisons of five different rectangular channels with parallel angled ribs. *International Journal of Heat and Mass Transfer*, 1992, **35,** 2891–2903.
8. Han, J. C., Zhang, Y. M. and Lee, C. P., Augmented heat transfer in square channels with parallel, crossed, and V-shaped angled ribs. *ASME Journal of Heat Transfer*, 1991, **113,** 590–596.
9. Han, J. C. and Zhang, Y. M., High performance heat transfer ducts with parallel, broken, and V-shaped ribs. *International Journal of Heat and Mass Transfer*, 1992, **35,** 513–523.
10. Kukreja, R. T., Lau, S. C. and McMillin, R. D., Local heat/mass transfer distribution in a square channel with full and V-shaped ribs. *International Journal of Heat and Mass Transfer*, 1993, **36,** 2013–2020.
11. Taslim, M. E., Li, T. and Kercher, D. M., Experimental heat transfer and friction in channels roughened with angled, V-shaped and discrete ribs on two opposite walls. *ASME Journal of Turbomachinery*, 1996, **118,** 20–28.
12. Liou, T. M. and Hwang, J. J., Turbulent heat transfer augmentation and friction in periodic fully developed channel flows. *ASME Journal of Heat Transfer*, 1992, **14,** 56–64.
13. Acharya, S., Dutta, S., Myrum, T. A. and Baker, R. S., Periodically fully developed flow and heat transfer in a ribbed duct. *International Journal of Heat and Mass Transfer*, 1993, **36,** 2069–2082.
14. Chandra, P. R., Niland, M. E. and Han, J. C., Turbulent flow heat transfer and friction in a rectangular channel with varying number of ribbed walls. ASME Paper No, 95-GT-13, 1995.
15. Boyle, R. J., Heat transfer in serpentine passages with turbulence promoters. ASME Paper No. 84-HT-24, 1984.
16. Han, J. C., Chandra, P. R. and Lau, S. C., Local heat/mass transfer distribution around sharp 180 degree turn in multipass rib-roughened channels. *ASME Journal of Heat Transfer*, 1988, **110,** 91–98.
17. Chandra, P. R., Han, J. C. and Lau, S. C., Effect of rib angle on local heat/mass transfer distribution in a two-pass rib-roughened channel. *ASME Journal of Turbomachinery*, 1988, **110,** 233–241.
18. Han, J. C. and Zhang, P., Effect of rib-angle orientation on local mass transfer distribution in a three-pass rib-roughened channel. *ASME Journal of Turbomachinery*, 1991, **113,** 123–130.
19. Chyu, M. K., Regional heat transfer in two-pass and three-pass passages with 180-deg sharp turns. *ASME Journal of Heat Transfer*, 1991, **113,** 63–70.
20. Ekkad, S. V. and Han, J. C., Local heat transfer distributions near a sharp 180° turn of a two-pass smooth channel using a transient liquid crystal image technique, *Journal of Flow Visualization and Image Processing*, 1995, **2,** 285–297.
21. Kline, S. J. and McClintock, F. A., Describing uncertainties in single-sample experiments. *Mechanical Engineering*, 1953, **75,** 3–8.